Methionine oxidation in α-synuclein inhibits its propensity for ordered secondary structure

Received for publication, January 16, 2018, and in revised form, January 30, 2019 Published, Papers in Press, February 12, 2019, DOI 10.1074/jbc.RA118.001907

Erika Ponzini[‡1], Antonella De Palma[§1], Lucilla Cerboni[‡], Antonino Natalello[‡], Rossana Rossi[§], Rani Moons[¶], Albert Konijnenberg[¶], Joanna Narkiewicz[‖], Giuseppe Legname[‖], Frank Sobott[¶‡‡], PierLuigi Mauri[§], Carlo Santambrogio[‡2], and Rita Grandori[‡3]**

*From the [‡]Department of Biotechnology and Biosciences, University of Milano-Bicocca, Piazza della Scienza 2, 20126 Milan, Italy, the [§]Institute of Biomedical Technologies, National Research Council of Italy, Segrate, 20090 Milan, Italy, the [¶]Biomolecular and Analytical Mass Spectrometry, University of Antwerp, Groenenborgerlaan 171, 2020 Antwerp, Belgium, the [‖]Department of Neuroscience, Scuola Internazionale Superiore di Studi Avanzati (SISSA) and ELETTRA-Sincrotrone Trieste S.C.p.A, 34136 Trieste, Italy, the [‡‡]School of Molecular and Cellular Biology, University of Leeds, Leeds LS29JT, United Kingdom, and the **Astbury Centre for Structural Molecular Biology, University of Leeds, Leeds LS2 9JT, United Kingdom*

Edited by Karen G. Fleming

α-Synuclein (AS) is an intrinsically disordered protein highly expressed in dopaminergic neurons. Its amyloid aggregates are the major component of Lewy bodies, a hallmark of Parkinson's disease (PD). AS is particularly exposed to oxidation of its methionine residues, both *in vivo* and *in vitro*. Oxidative stress has been implicated in PD and oxidized α-synuclein has been shown to assemble into soluble, toxic oligomers, rather than amyloid fibrils. However, the structural effects of methionine oxidation are still poorly understood. In this work, oxidized AS was obtained by prolonged incubations with dopamine (DA) or epigallocatechin-3-gallate (EGCG), two inhibitors of AS aggregation, indicating that EGCG promotes the same final oxidation product as DA. The conformational transitions of the oxidized and non-oxidized protein were monitored by complementary biophysical techniques, including MS, ion mobility (IM), CD, and FTIR spectroscopy assays. Although the two variants displayed very similar structures under conditions that stabilize highly disordered or highly ordered states, differences emerged in the intermediate points of transitions induced by organic solvents, such as trifluoroethanol (TFE) and methanol (MeOH), indicating a lower propensity of the oxidized protein for forming either α- or β-type secondary structures. Furthermore, oxidized AS displayed restricted secondary-structure transitions in response to dehydration and slightly amplified tertiary-structure transitions induced by ligand binding. This difference in susceptibility to induced folding could explain the loss of fibrillation potential observed for oxidized AS. Finally, site-specific oxidation kinetics point out a minor delay in Met-127 modification, likely due to the effects of AS intrinsic structure.

This work was supported by the Fondazione Regionale per la Ricerca Biomedica (FRRB-Regione Lombardia), a grant from the University of Milano-Bicocca (FAR - Fondo di Ateneo per la Ricerca), and the EU COST Action BM1403. The authors declare that they have no conflicts of interest with the contents of this article.
This article contains Figs. S1–S5 and Tables S1 and S2.
[1] Both authors contributed equally to this work.
[2] To whom correspondence may be addressed. Tel.: 39-02-64483458; E-mail: carlo.santambrogio@unimib.it.
[3] To whom correspondence may be addressed. Tel.: 39-02-64483363; E-mail: rita.grandori@unimib.it.

α-Synuclein (AS)[4] is a 140-residue, intrinsically disordered protein (IDP) (1) highly expressed in the presynaptic nerve terminals, where it plays a regulatory role in synaptic homeostasis (2–4). Three regions can be recognized in its primary structure: the N-terminal region, capable to bind membranes undergoing coil-to-helix transitions; the central, hydrophobic region involved in amyloid fibril formation; and the C-terminal, acidic region responsible for pH-dependent conformational transitions and binding to multiple protein interactors. AS aggregation is a hallmark of PD and related neurodegenerative disorders. Aggregated AS is the major component of Lewy bodies and AS mutations or altered expression correlate with increased risk of PD onset (4).

AS oxidation has been long implicated in PD. However, the underlying molecular mechanisms are not clear yet. Due to the oxidative challenge represented by DA, dopaminergic neurons are particularly exposed to protein oxidative damage. AS can be oxidized on its four methionine residues (positions 1, 5, 116, and 127), *in vivo* and *in vitro* (5). Typical effective oxidants are DA, via its oxidation products, and H_2O_2 (6–9). Methionine-oxidized AS is inhibited in fibrillation and, rather, aggregates into soluble, SDS-resistant oligomers with variable degrees of cytotoxicity (9–12). Methionine sulfoxide epimers can be enzymatically reduced *in vivo* by the activity of methionine sulfoxide reductase (13). In-cell NMR, however, has shown that only Met-1 and Met-5 are restored in oxidized AS, whereas C-terminal positions 116 and 127 are not targeted by the cellular repair machinery in mammalian cells, which could lead to the accumulation of toxic species (14).

Protein oxidation on methionine residues to give sulfoxide is thought to affect protein function mainly via structural effects (5). The modification causes, indeed, a remarkable loss of hydrophobic character of the methionine side chain, which could affect secondary and tertiary structure (7). Furthermore,

[4] The abbreviations used are: AS, α-synuclein; CCS, collision cross-section; DA, dopamine; DHA, docosahexaenoic acid; EGCG, epigallocatechin-3-gallate; ESI-MS, electrospray ionization-mass spectrometry; IDP, intrinsically disordered protein; IM, ion mobility; MeOH, methanol; $oMet_0$ AS, fully reduced α-synuclein; $oMet_4$ AS, fully oxidized α-synuclein; PD, Parkinson disease; TFE, 2,2,2-trifluoroethanol.

methionine oxidation results in a lower intrinsic propensity for helical structures as shown on poly-Met polymers (15). To interpret the biological responses to AS oxidation, it is important to understand the effect of methionine oxidation *per se* on AS conformational transitions, dissecting it from other, frequently associated processes like protein–protein and protein–membranes interactions or other AS covalent modifications.

Based on CD spectroscopy, fully oxidized ($oMet_4$) AS appears to be slightly more disordered than non-oxidized ($oMet_0$) AS, with very minor losses of intrinsically formed helical segments (7). However, the spectra are almost superimposable and imprinted to a general character of highly disordered protein (7, 14, 16). On the other hand, both proteins are highly helical in the presence of a strong molar excess of docosahexaenoic acid (DHA), with $oMet_4$ AS displaying a similar helical content as $oMet_0$ AS (17). Nevertheless, a conceivable hypothesis is that oxidation impacts on AS propensity to acquire ordered secondary/tertiary structure (7). Such a mechanism could be at the basis of different propensities of reduced and oxidized AS to populate the amyloidogenic conformer that triggers fibrillation. An indication of different conformational transitions of the two protein variants derives from NMR analysis of the helicity induced by N-terminal acetylation in the first 10 residues of the protein. The comparison of $oMet_4$ and $oMet_0$ AS indicates that oxidation inhibits the acetylation-induced conformational transition in the N-terminal residues (18).

This work focuses on the characterization of AS oxidation products to test the hypothesis that methionine oxidation affects AS conformational transitions, despite the similar secondary structure displayed by $oMet_4$ and $oMet_0$ AS in highly disordered or highly helical states. Oxidation is monitored upon prolonged incubations with DA or EGCG. Both ligands inhibit AS fibrillation and induce formation of oligomers (10, 19), which are not toxic in the case of EGCG (19). The two ligands bind AS with distinct conformational selectivity, forming noncovalent and non-oxidized complexes upon short incubation time (20). However, it has been shown that AS can be oxidized by DA (9, 10), and other proteins by EGCG (21), after a long incubation time. Here, AS oxidation is monitored by electrospray ionization MS (ESI-MS) and the monomeric, soluble, fully oxidized product is analyzed by CD, FTIR spectroscopy, and native MS, under conditions that promote either α- or β-type secondary structure.

Results

Oxidation kinetics

AS susceptibility to covalent modifications in the presence of DA or EGCG has been investigated by incubating the protein with either ligand at 37 °C under mild agitation. 2 mM DA and 200 μM EGCG were used as previously characterized conditions enabling effective detection of AS-ligand noncovalent complexes (20). Aliquots were taken at different time points, purified from salts and free ligand, and analyzed by ESI-MS under denaturing conditions for intact protein detection. The data reported in Fig. 1, *A–C*, show that, under prolonged incubation, both ligands induce stepwise mass shifts of 16 Da in AS peaks, corresponding to progressive oxidation states. Up to 4 oxidations per AS molecule can be detected, which correspond to the number of methionine residues in the molecule. The species distributions evolve toward an almost homogeneous, 4-oxidized population after 72 h, with still ~10% of 3-oxidized protein detectable in the presence of DA and ~20% in the presence of EGCG (Fig. 1, *D* and *E*). No covalent adducts with the ligands are detectable under these conditions. These results indicate that both ligands can induce AS oxidation.

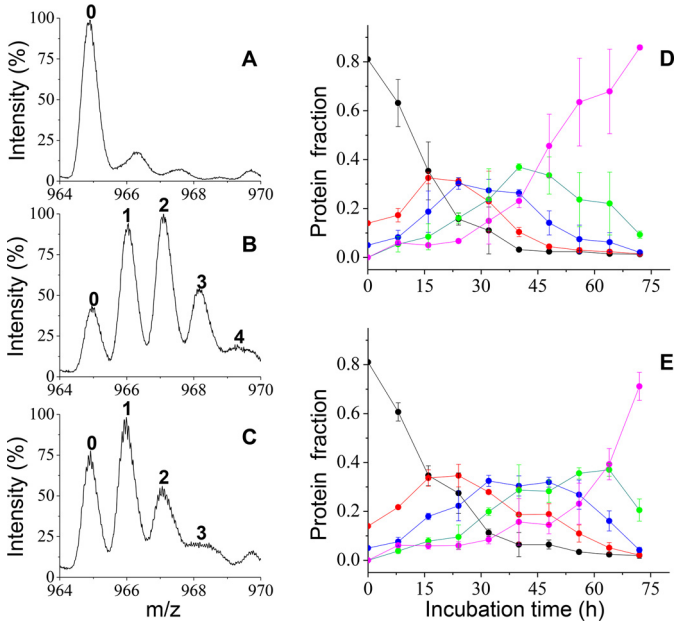

Figure 1. Oxidation kinetics of intact AS. *A–C*, ESI-MS peaks corresponding to the 15+ charge state of AS after a 24-h incubation in the absence of ligands (*A*), in the presence of DA (*B*), and in the presence of EGCG (*C*). In each panel the peaks are labeled by the number of oxidized residues. (*D* and *E*): AS oxidation extent (0, *black*; 1, *red*; 2, *blue*; 3, *green*; 4, *magenta*, oxidized methionine residues) as a function of the incubation time in the presence of DA (*D*) or EGCG (*E*). *Error bars* indicate the standard deviation from three independent experiments.

To map the modification sites and describe their individual kinetics, chymotryptic peptides from the same samples as above were analyzed by ESI-MS (Fig. 2). Three oxidized methionine residues (positions 1, 116, and 127, Table S1) were identified in samples incubated with either DA or EGCG by ESI-MS/MS, indicating that the modification corresponds to sulfoxidation (Fig. S1). Likely, the fourth modification involves the peptide containing Met-5, which could not be identified in either oxidized or non-oxidized forms and is presumably lost during the purification procedure, due to its very small size. Quantification of the oxidation extent was obtained by the peak–height ratios between the oxidized and non-oxidized forms of each detected peptide (Fig. 2, *A–C*, and Fig. S2).

To retrieve direct evidence on the oxidation state of all four methionine residues, tryptic digests were analyzed as well (Fig. 2). This procedure generates an N-terminal peptide containing Met-1 and Met-5 and a C-terminal peptide containing Met-116 and Met-127. The extent of oxidation at positions 1 and 5 could be assessed from the MS/MS data, as the ratio between peptide spectrum matches of the oxidized and non-oxidized form of the N-terminal peptide (Fig. 2, Figs. S3–S5, and Table S1). The use of the MS/MS spectral counts method in place of the MS precursor–ion peak–height made it possible to exactly calcu-

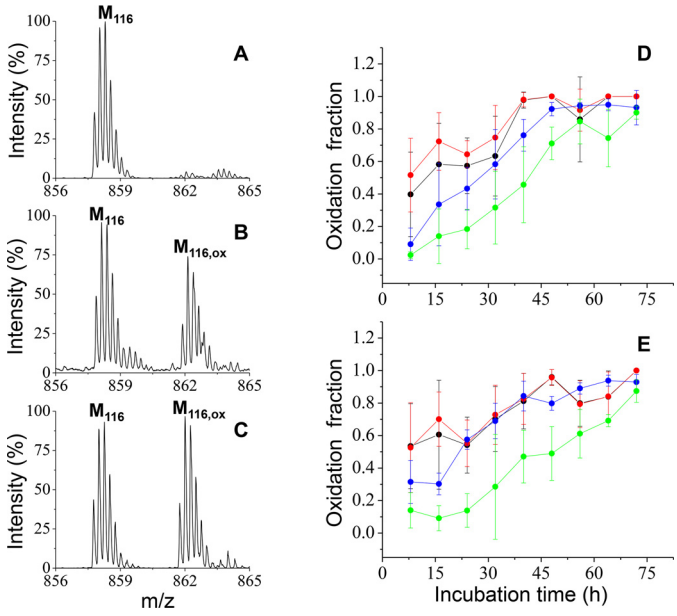

Figure 2. Oxidation kinetics of AS methionine residues. *A–C*, ESI-MS peaks corresponding to the 4+ charge state of the AS chymotryptic peptide containing Met-116, after 24-h incubation in the absence of ligands (*A*), in the presence of DA (*B*), and in the presence of EGCG (*C*). *D* and *E*, oxidation fraction of each methionine residue (M_1, *black*; M_5, *red*; M_{116}, *blue*; M_{127}, *green*) as a function of the incubation time in the presence of DA (*D*) or EGCG (*E*). Quantification for Met-116 and Met-127 has been performed on MS data on chymotryptic peptides. Quantification for Met-1 and Met-5 has been performed on MS/MS data on tryptic peptides. The *black* and *red symbols* are mostly overlaid for the 40-h time point and beyond. *Error bars* indicate the S.D. from at least three independent experiments.

late the contribution of single oxidation events on either Met-1 or Met-5, thus enabling measurement of the oxidation rate of individual methionine residues (Fig. S5). This would not be possible using peak–height or peak–area calculations on the precursor ion, because the latter has the same *m/z* value whether the single oxidation concerns Met-1 or Met-5. The C-terminal tryptic peptide, instead, is too large to yield high-quality MS/MS spectra by collision-induced dissociation, hindering accurate sequence assignment and quantification of the oxidation levels. Thus, the extent of oxidation at positions 116 and 127 was better calculated from MS data of the respective chymotryptic peptides (Fig. 2, *A–C*, Fig. S2). The list of the identified peptides by tryptic and chymotryptic digestions is reported in Table S1.

The resulting, position-specific oxidation profiles are reported in Fig. 2, *D* and *E*. It can be noticed that oxidation kinetics at positions 1, 5, and 116 are quite similar and reach a plateau around 40 h incubation under the conditions employed here, with either ligand. Oxidation of Met-127, instead, is slightly but systematically delayed relative to the others. It is interesting to note that this residue belongs to the ^{125}YEMPS^{129} motif, which has been implicated in long-range interactions with the central NAC (non-amyloid-β component) region and interaction with DA and its oxidation products (22–26). These local structural features are likely at the basis of the different oxidation kinetics of the Met-127 residue.

Secondary-structure transitions

The conformational response of $oMet_0$ and $oMet_4$ AS to organic solvents has been studied by far-UV CD. Under non-denaturing conditions, the two species display a typical spectra of intrinsically disordered proteins, characterized by a large amount of random coil (minimum at 200 nm), with a small α-helical component (shoulder at 222 nm) (7) (Fig. 3*A*). The addition of either TFE (Fig. 3, *B* and *C*) or MeOH (Fig. 3, *E* and *F*) induces, respectively, the acquisition of α- or β-type secondary structures by $oMet_0$, as previously described (27). Under the same conditions, oMet4 AS displays a lower propensity to form ordered secondary structure relative to $oMet_0$ AS, with higher concentrations of organic solvent being required to observe similar effects. Moreover, the final secondary structure displayed by the two proteins at high solvent concentrations (15% TFE and 40% MeOH), which correspond to the post-transition spectra of $oMet_0$ AS (27), are not identical. In both cases, $oMet_4$ AS shows a lower content of ordered secondary structure, particularly in the case of methanol-induced β-strands, as indicated by the lower intensity of the signal at 215 nm.

AS incubation in the presence of DA is known to induce formation of soluble, SDS-resistant oligomers. SDS-PAGE analysis indicates that higher-order species are detectable, particularly upon EGCG treatment. Their amount in the samples used here for CD titrations (Fig. 3*D*) is below 15%, as assessed from densitometry analysis (data not shown). The absence of bands in the pellet lanes of the gel rules out the presence of aggregates that become soluble in SDS and the comparable intensity of monomeric AS suggests that no significant amount of material is lost in the pellet of the final sample clarification after SDS solubilization. Some faint bands (~8%) can be detected at slightly lower molecular weight, likely due to some proteolytic degradation. In conclusion, the observed structural features can be ascribed to soluble, monomeric AS, which is the largely predominant species in the analyzed samples. Dynamic equilibrium with SDS-sensitive oligomeric species cannot be ruled out, although it has not been described before, for AS under similar conditions.

Secondary structure of $oMet_0$ and $oMet_4$ AS has been analyzed also by FTIR spectroscopy. The absorption and second-derivative spectra of AS samples, measured in the form of protein films, are reported in Fig. 4, *A* and *B*, for the Amide I band, which is mainly due to the stretching vibration of the peptide bond (28). The main spectral component around 1657 cm^{-1} can be assigned to random coil with possible contribution of α-helical structures. Two additional peaks are evident around 1696 and 1627 cm^{-1}. In agreement with a previous study, these peaks can be assigned to β-sheet structures induced by solvent evaporation and protein–protein interactions in the film (29). The $oMet_4$ protein displays a lower intensity of such component (Fig. 4, *A* and *B*), indicating a lower content of ordered β-structures compared with $oMet_0$ AS.

The secondary structure of $oMet_0$ and $oMet_4$ AS has also been studied here by conventional FTIR measurements of the proteins in D_2O solution (30, 31). The Amide I absorption and second-derivative spectra of the two proteins in solution at 30 °C were superimposable (Fig. 4, *C* and *D*) and were characterized by a main component around 1642 cm^{-1} assigned to random-coil structures (27–29, 32). These data for the protein in solution are only in apparent contrast with those on protein films and can be interpreted by a role of dehydration in the

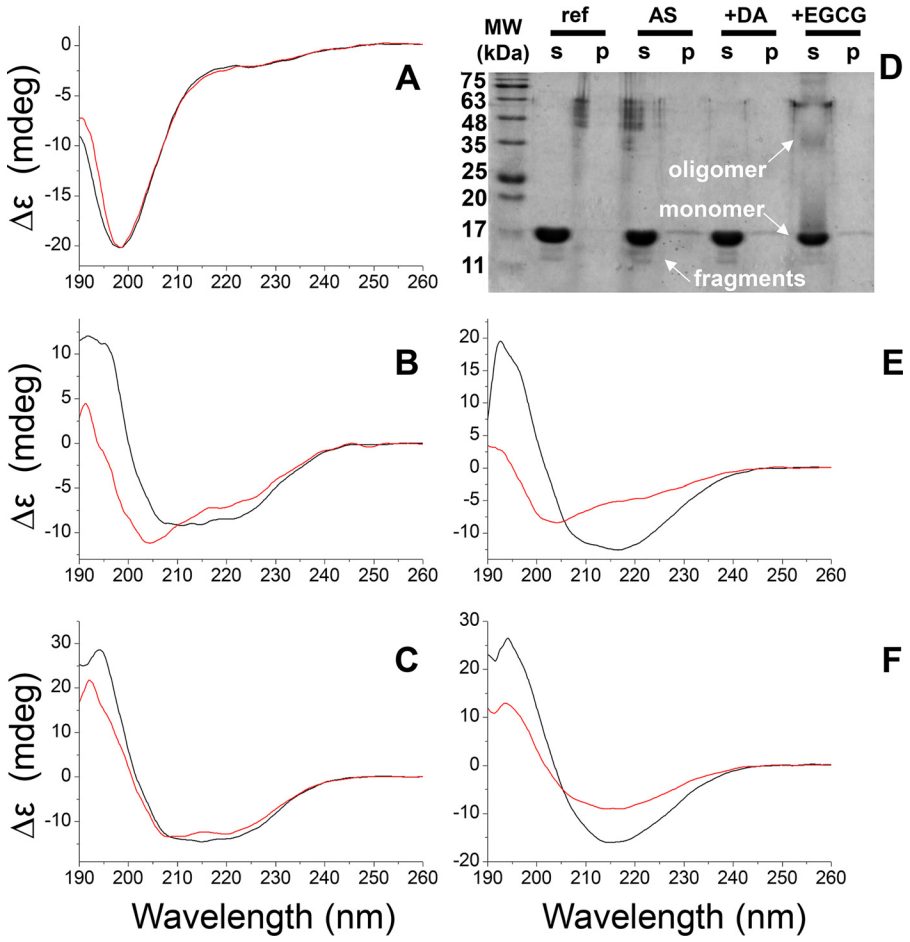

Figure 3. Secondary-structure transitions by CD spectroscopy. Far-UV CD spectra of $oMet_0$ (*black lines*) and $oMet_4$ (*red lines*) AS in the absence of organic solvents (*A*); in the presence of 10% (*B*) and 15% (*C*) TFE; in the presence of 35% (*E*) and 40% (*F*) MeOH. *D,* SDS-PAGE analysis of supernatants (*s*) and pellets (*p*) obtained from the following samples: AS before incubation (*ref*); AS after 72 h incubation in the absence of ligands (AS); AS after 72 h incubation in the presence of DA (+DA); AS after 72 h incubation in the presence of EGCG (+EGCG). The bands corresponding to AS monomer, fragments, and oligomers are labeled. Representative data from at least three independent experiments are shown.

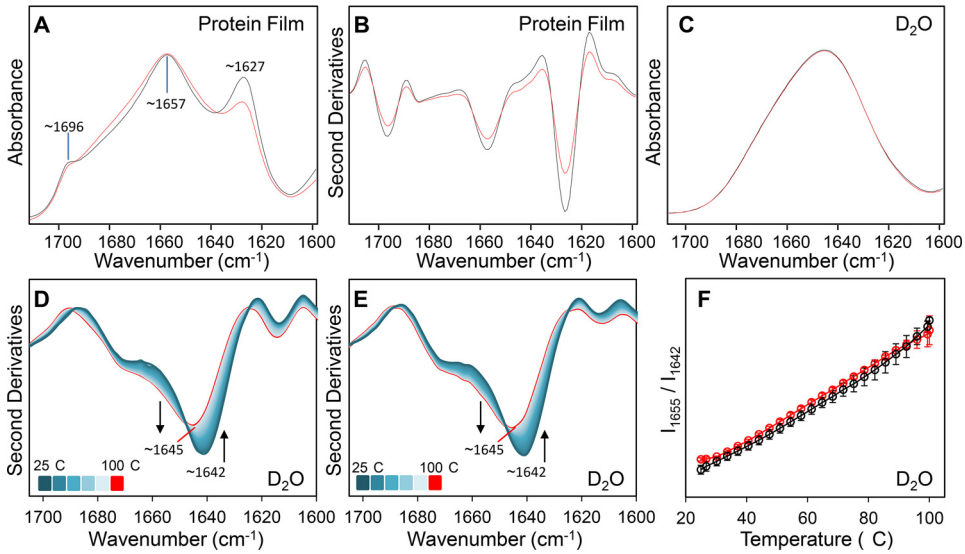

Figure 4. Secondary-structure transitions by FTIR spectroscopy. Absorption (*A*) and second-derivative (*B*) spectra of $oMet_0$ (*black lines*) and $oMet_4$ (*red lines*) AS measured in the form of protein films obtained after solvent evaporation. *C,* absorption spectra of $oMet_0$ and $oMet_4$ AS measured in D_2O solution at 30 °C. Second-derivative spectra of $oMet_0$ (*D*) and $oMet_4$ (*E*) AS measured in D_2O solution at different temperatures from 25 to 100 °C. *Arrows* point to the spectral changes observed at increasing temperatures. The peak positions of the main components are shown. *F,* ratio of the intensity at 1655 and 1642 cm^{-1} taken from the second-derivative spectra of *D* and *E*. Representative data from 3 (*A* and *B*) or 2 (*C–F*) independent experiments are shown. *Error bars* indicate the standard deviation.

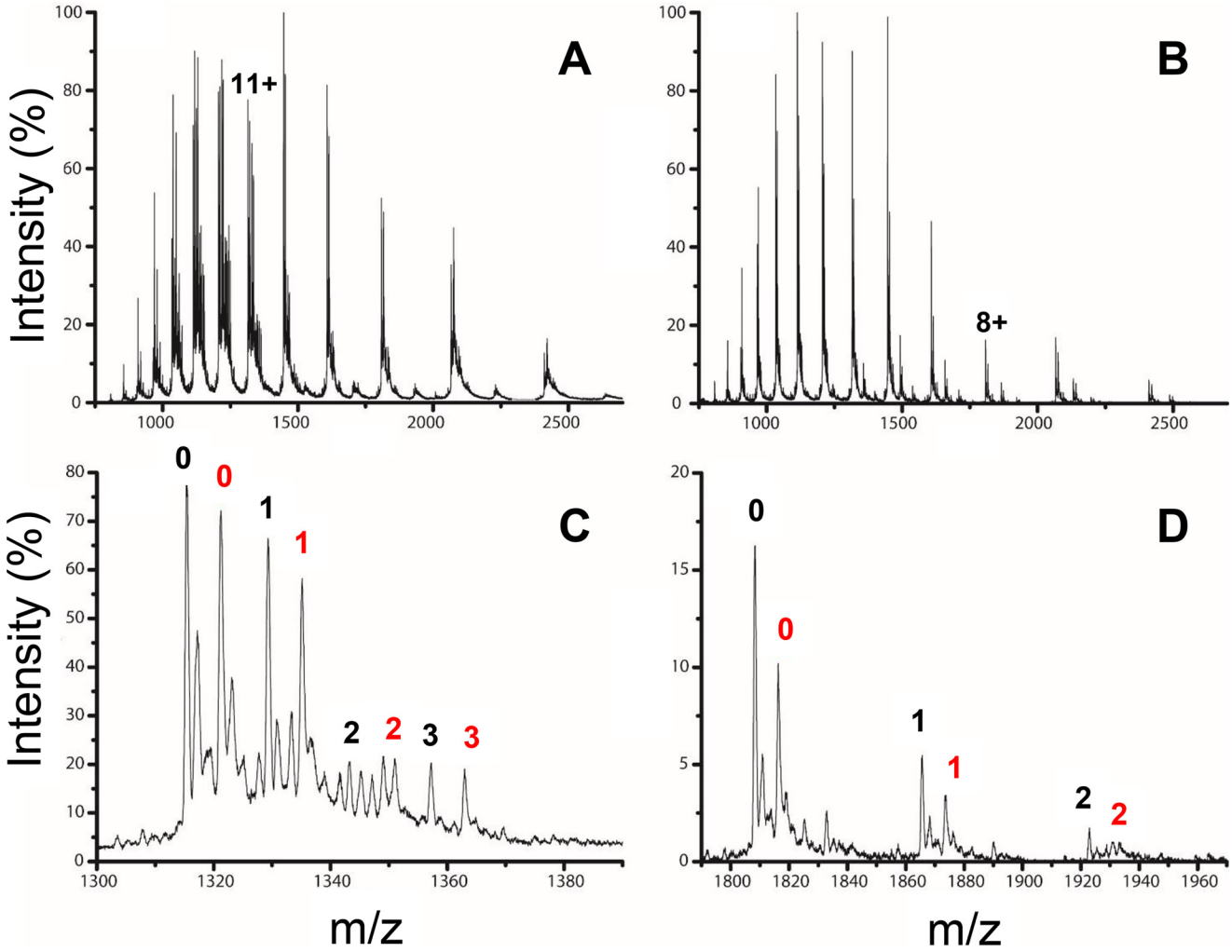

Figure 5. Ligand binding by native MS. *A* and *B*, ESI-MS spectra of ternary mixtures of $oMet_0$, $oMet_4$, and either DA (*A*) or EGCG (*B*). The 11+ and 8+ peaks are labeled by the corresponding charge state. *C* and *D*, magnification of *A* and *B* in the region of the 11+ (*C*) and 8+ (*D*) charge state. The peaks of $oMet_0$ (*black symbols*) and $oMet_4$ (*red symbols*) are labeled by the number of ligand molecules bound in the complex. Representative data from at least three independent experiments are shown.

observed response of semidry $oMet_4$. Thus, oxidation *per se* is not enough to induce major changes in AS secondary structure in solution but it reduces its propensity to form ordered structure, as those induced by dehydration.

The conformational stability has been compared by applying temperature ramps. The spectral changes induced by heating the protein solutions from 25 to 100 °C are very similar for $oMet_0$ and $oMet_4$ AS (Fig. 4, *D–F*). Therefore, FTIR analyses detect comparable secondary structure and temperature response for $oMet_0$ and $oMet_4$ AS in D_2O solution (Fig. 4, *C–F*). It has been pointed out that such spectral changes of IDPs could also be interpreted as a loss of polyproline II-like structures, rather than acquisition of α-helices (33).

In conclusion, conformational properties of $oMet_0$ and $oMet_4$ AS are very similar, as assessed by CD and FTIR. However, both techniques can capture differences under particular conditions, always in the direction of a reduced propensity of $oMet_4$ to acquire ordered secondary structure.

Ligand binding

Native MS has been employed to evaluate the effects of oxidation on ligand binding by AS. Ternary mixtures of $oMet_0$, $oMet_4$, and either DA or EGCG have been analyzed by ESI-MS under nondenaturing conditions, allowing for comparison under identical conditions and direct protein competition for the same ligand. The spectra reveal complexes for each protein form, which can be distinguished by their distinct masses (Fig. 5). Ligand binding displays the same stoichiometry and the same conformational selectivity for the two protein variants, with preferential binding of DA to more extended conformations (charge states 10+ to 14+) and EGCG to more compact forms (charge states 6+ to 12+), as already reported for the non-oxidized protein (20). The apparent affinities of DA for $oMet_0$ and $oMet_4$ seem to be comparable, too, because the amounts of complexes at each binding step are very similar (as seen for the 11+ and 8+ charge states in Fig. 5, *C* and *D*). The latter has been chosen as the ion with the highest fraction of bound EGCG. The 11+ charge state for DA complexes has been selected as the lowest charge state with significant ligand bound, to prevent conformational artifacts induced by Coulomb repulsions that can contribute to higher charge states (20). These peaks are used for further analysis of the protein–ligand complexes.

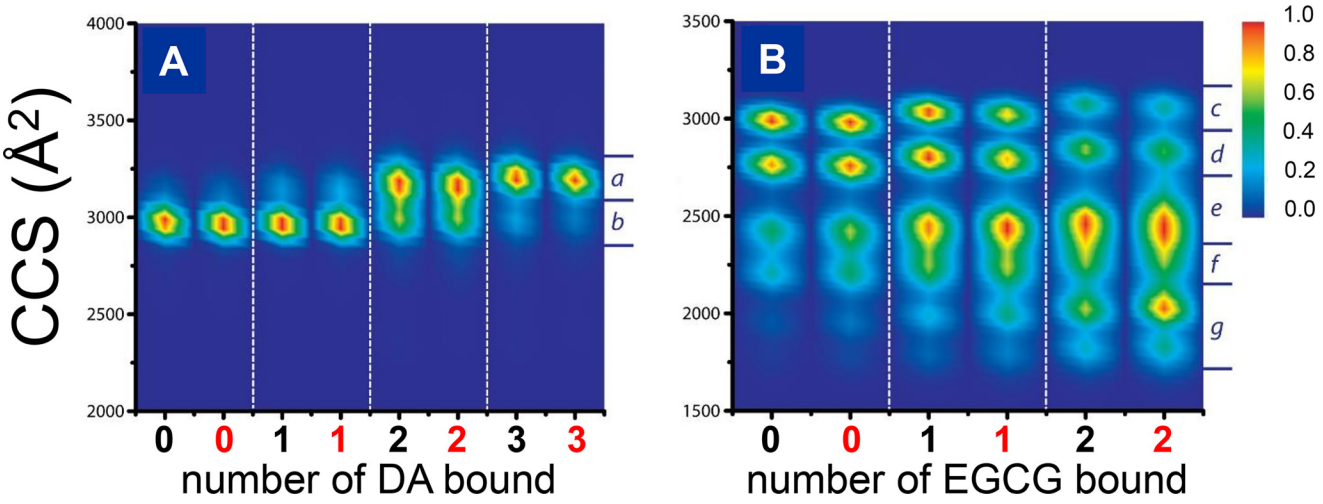

Figure 6. Tertiary-structure transitions induced by ligand binding to AS by IM-MS. Collision cross-section obtained from the 11+ (*A*) or 8+ (*B*) charge states of $oMet_0$ and $oMet_4$ complexes with ligands by IM-MS experiments, as a function of the number of bound ligand molecules ($oMet_0$, *black symbols*; $oMet_4$, *red symbols*). The relative intensities of the signals are expressed by a color scale (*inset*). Conformers are named by *lowercase, italic letters*. Representative data from at least three replicas are shown.

To obtain a more detailed description of structural compactness, the collision cross-section (CCS) of the protein and its noncovalent complexes has been measured by nano-ESI ion mobility (IM) MS and shown in Fig. 6. The observed segregation of DA and EGCG complexes in the charge state diffusion reflects the previously reported (20) conformational selectivity of the two different ligands. Multiple conformers with slightly different compactness are distinguishable, even within the same charge state.

For the 11+ charge state (Fig. 6*A*), the free protein populates almost exclusively the more compact conformer (*b*), irrespective of the oxidation state. As already shown previously (20), DA binding stabilizes the more extended conformer (*a*), giving larger CCS. The more DA molecules bound, the higher the relative population of the *a* conformer. This effect is maintained in the oxidized protein variant, with minor differences. A small amplification of the effect can be observed in the oxidized form, with slightly larger fractions of the extended form detectable (Fig. 6). The effect, however, is barely significant (Table S2).

The results for the 8+ charge state show at least five different conformers (*c*–*g*), consistent with an ensemble also featuring collapsed forms (Fig. 6*B*). Oxidation seems to affect species distributions whether or not EGCG is bound. Even in the free protein, the compact states below 2500 $Å^2$ CCS are slightly enriched in $oMet_4$ relative to $oMet_0$. As previously described (20), EGCG binding to AS promotes formation of these compact conformers (*e*–*g*). Oxidation amplifies such an effect, with slightly larger fractions of the collapsed species detectable at each stoichiometry (Fig. 6, Table S2).

Thus, oxidation seems to play subtle effect in AS tertiary-structure transitions induced by ligands, with a slight amplification of the effects seen for the non-oxidized protein. The difference, however, is only in the relative amounts of the different conformers and not, apparently, in their structure.

Discussion

Several lines of evidence suggest that DA inhibition of AS fibrillation is mediated by methionine oxidation (8). In this work it is shown that EGCG, another ligand with inhibitory effects (19), induces methionine oxidation in AS, strengthening the hypothesis that accumulation of $oMet_4$ AS plays a central role controlling the pathways of AS amyloid aggregation. The oxidative effects of DA and EGCG seem to be due to production of H_2O_2 in the presence of oxygen and further accumulation of the hydroxyl radical by the Fenton reaction in the presence of even traces of Cu^+ or Fe^{2+} (5, 34). In addition, distinct effects on AS conformation are induced by the formation of noncovalent complexes with DA and EGCG, with the stabilization of different protein conformers upon ligand binding (20). These ligand-specific effects could be responsible of further differences in the type of the predominant aggregation products.

Oxidative modifications induced by EGCG have been described for other proteins (21), although apparently contrasting evidence is reported in the literature. Indeed, EGCG displays both antioxidant and pro-oxidant effects under different environmental conditions (21). *In vitro* assays have shown that EGCG is capable to scavenge different reactive species, such as the superoxide anion and hydroxyl radicals (35). On the other hand, the EGCG autoxidation can generate EGCG radical, superoxide radical, and hydrogen peroxide species (34, 36). It has been reported that one molecule of EGCG can produce about two molecules of hydrogen peroxide after overnight incubation in phosphate buffer, pH 7, at a concentration of 0.022–0.22 mM (36). The different effects reported in the literature might be interpreted in terms of EGCG concentration relative to oxygen partial pressure (21). Although DA and EGCG have distinct AS-binding properties in terms of affinity, conformational selectivity, and conformational effects (20), protein modification by the two ligands takes place with only minor differences in the kinetics of the individual methionine residues, in line with a mechanism involving H_2O_2 production

in the presence of either ligand. This is consistent with the fact that AS incubation with H_2O_2 results in the same covalent modifications as those reported here (data not shown) (37).

$oMet_4$ AS is endowed with a strongly reduced propensity to form amyloid fibrils relative to $oMet_0$ (7). It has been suggested that this feature might derive from a reduced tendency to form a β-type secondary structure. However, $oMet_0$ and $oMet_4$ AS display very similar structural properties, as assessed by various spectroscopic methods under several different conditions (7, 14, 16, 17). The same has been reported here for the highly helical conformation at high TFE concentrations, the β-rich state in the presence of high MeOH concentrations, and the highly disordered state in aqueous buffers in the absence of ligands. Furthermore, the thermal stability of the intrinsic structural elements of the two protein variants is very similar. On the other hand, the CD results reported here show that differences emerge at intermediate points of the titrations with TFE and MeOH, in which the oxidized protein consistently displays a higher disorder content than unmodified AS. Such a trend is in agreement with FTIR data, showing restricted response to dehydration. The latter condition has been already shown to induce formation of intermolecular β-sheets (29).

At the tertiary-structure level, oxidized AS displays slight amplification of ligand-induced conformational changes, particularly with EGCG. This ligand stabilizes AS-collapsed conformations, as shown by IM-MS, and this effect is more remarkable in the oxidized protein. This behavior could seem in contrast with the reduced chain flexibility caused by methionine oxidation (38). This result suggests that the change in side chain chemical properties is the most relevant effect of oxidation and hints, in turn, to a predominant role of polar interactions mediating chain compaction in the presence of this polyphenolic ligand.

The lower propensity of $oMet_4$ AS to acquire ordered secondary structure, and particularly β-sheets, is relevant in the context of AS amyloid aggregation and could explain the inhibition of fibrillation potential by methionine oxidation. Indeed, fibrils, on-pathway oligomers, and off-pathway oligomers are characterized by different type and content of secondary-structure elements (16, 39). Even minor differences in the relative stability of alternative conformers could strongly affect the evolution of ensembles governed by competing pathways.

Experimental procedures

Chemicals and proteins

Ammonium acetate, ammonium hydroxide, DA, EGCG, acetonitrile, formic acid, acetic acid, chymotrypsin, ammonium bicarbonate, monosodium phosphate, disodium phosphate, TFE, and MeOH were purchased from Sigma. WT human AS without any tag (average mass 14460.1 Da) was expressed in recombinant form and purified as previously described (40).

AS oxidation analysis by ESI-MS

Samples containing 70 μM AS were incubated at 37 °C in 50 mM ammonium acetate, pH 7.0, under mild agitation (400 rpm) in the presence of 2 mM DA or 200 μM EGCG (20). Aliquots were taken every 8 h for 3 days, purified from salts and ligands by reversed-phase chromatography (Zip Tip C4 Millipore, Burlington, MA), and analyzed by ESI-MS to determine AS oxidation levels. Part of the purified aliquots were frozen, dried, and resuspended for in-solution digestion by chymotrypsin (Sigma). Digestion were carried out at 1:50 enzyme:substrate ratio (w/w), in 50 mM ammonium bicarbonate, and incubation at 37 °C for 18 h. The resulting peptides were desalted by Zip Tip C18 (Millipore) and analyzed by ESI-MS and ESI-MS/MS, to map modifications and monitor oxidation kinetics.

MS spectra of intact protein or chymotryptic peptides were collected in positive-ion mode, using a hybrid quadrupole-TOF mass spectrometer (QSTAR-Elite, AB Sciex, Foster City, CA) equipped with a nano-ESI source. Samples were infused at room temperature by metal-coated borosilicate capillaries (Thermo Fisher Scientific, Waltham, MA) with a medium-length emitter tip of 1-μm internal diameter. The main instrumental parameters were set as follows: ion spray voltage, 1.1–1.2 kV; declustering potential, 100 V; curtain-gas pressure, 20 p.s.i. Final spectra were obtained by averaging the signal over 2 min acquisition. All the data were processed using Analyst QS 2.0 (AB Sciex) software. Oxidation ratios for chymotryptic peptides were calculated as ratios between the peptide peak–height in MS spectra.

Trypsin (Promega, Madison, WI) digestion was performed at 1:50 enzyme:substrate ratio (w/w), in 100 mM ammonium bicarbonate, and incubation at 37 °C for 18 h. Trypsin-digested mixtures were analyzed by the Eksigent nanoLC-Ultra 2D System (Eksigent, AB SCIEX, Dublin, CA) on a nanoLC column (75 μm × 15 cm 3C18-CL, 3 μm, 120 Å), through a 35-min gradient of 5–60% of eluent B (eluent A, 0.1% formic acid in water; eluent B, 0.1% formic acid in acetonitrile), at a flow rate of 300 nl/min. Mass spectra were acquired using a LTQ-Orbitrap XL-ETD mass spectrometer (Thermo Fisher Scientific, San José, CA), equipped with a nanospray ionization source. Nanospray was achieved using a coated fused silica emitter (New Objective, Woburn, MA) (360 μm outer diameter/50 μm inner diameter; 730 μm tip inner diameter) held at 1.6 kV. The ion transfer capillary was held at 220 °C. Full mass spectra were recorded in positive ion mode over a 400–1600 m/z range and with a resolution setting of 30,000 FWHM and scan rate of 2 spectra/s, followed by five low-resolution MS/MS events, sequentially generated in a data-dependent manner on the top five most intense ions selected from the full MS spectrum, using dynamic exclusion for MS/MS analysis. All data generated were searched using the Sequest HT search engine contained in the Thermo Scientific Proteome Discoverer software, version 2.1. Methionine oxidation was set as dynamic modification. Oxidation extent was calculated as the ratio between peptide spectrum matches of the oxidized and non-oxidized forms. This method counts the number of MS/MS spectra identified for a given peptide and, consequently, its relative abundance, in each analyzed condition.

AS secondary structure by CD and FTIR

$oMet_4$ AS and $oMet_0$ AS were buffer-exchanged by *Zeba Spin* desalting columns (Thermo Fisher Scientific) with elution in 50 mM sodium phosphate, pH 7.0. CD spectra in the far-UV range (190–260 nm) were acquired on a J-815 spectropolarimeter (JASCO Corp., Tokyo, Japan), equipped with a Peltier sys-

tem for temperature control. Samples were clarified by centrifugation at 10,000 × *g* and measured in 50 mM sodium phosphate, pH 7.0, in the presence of variable amounts of TFE or MeOH, employing a protein concentration of 10 μM and quartz cuvette of 1-mm path length. The following instrumental settings were applied: data pitch, 0.1 nm; scan speed, 20 nm/min; bandwidth, 1 nm; accumulation spectra, 2.

For FTIR analyses, the $oMet_0$ and $oMet_4$ AS samples were measured in the form of a semidry film or in D_2O solution. In particular, 2 μl of AS samples at 5 mg/ml of protein concentration in 50 mM sodium phosphate, pH 7.0, were deposited on a BaF_2 window and dried at room temperature, to obtain a solid film. The FTIR absorption spectra were then acquired in transmission mode by means of a Varian 670-IR FTIR spectrometer coupled to the Varian 610-IR IR microscope (both from Varian, Mulgrave VIC, Australia Pty. Ltd.) (41), under the following instrumental settings: 2 cm^{-1} spectral resolution, 25 kHz scan speed, 512 scan co-additions, triangular apodization, mercury cadmium telluride nitrogen-cooled detector, and a variable aperture of the microscope of 100 μm × 100 μm. Considering that the total amount of protein can still be different even within a fixed surface area, due to variability in film thickness, we compared only spectra of $oMet_0$ and $oMet_4$ AS with similar Amide I areas. Because solvent evaporation can induce protein conformational changes and aggregation (29), it is particularly important to compare samples with similar protein contents. For conventional transmission-mode measurements of the proteins in D_2O solutions (30, 31), lyophilized $oMet_0$ and $oMet_4$ AS samples were resuspended in deuterated 50 mM sodium phosphate, pH 7.0, at a protein concentration of 5 mg/ml. A sample volume of 20 μl was placed in a temperature-controlled transmission cell with two BaF_2 windows separated by a 100-μm Teflon spacer and the spectra were collected using the Varian 670-IR FTIR spectrometer as described above. To increase the signal-to-noise ratio, 1,000 scan co-additions were employed. FTIR spectra were collected during the thermal treatment of the protein solutions from 25 to 100 °C at a heating rate of 0.4 °C/min. Protein absorption was obtained after subtraction of solvent absorption, measured under the same conditions. The FTIR spectra were baseline-corrected and the subtraction of residual vapor signals was also performed when necessary (31). All the absorption spectra were normalized for the Amide I band area. Second-derivative spectra were obtained after the smoothing of the measured spectra by the Savitzky Golay algorithm (42). Data collection and analysis were performed using the Resolutions-Pro software (Varian, Mulgrave VIC, Città, Australia Pty. Ltd.).

SDS-PAGE

Samples after the 72-h incubation were centrifuged for 10 min at 10,000 × *g* to separate soluble and insoluble protein fractions. Pellets were resuspended into a volume identical to the supernatant (40 μl), and 6 μl of each fraction were run on 14% PAGE on a mini-gel apparatus (Bio-Rad), according to the Laemmli protocol for SDS-PAGE (43) and stained by SimplyBlu SafeStain (Life Technologies).

Ligand binding by native MS and IM-MS

$oMet_4$ AS was obtained by incubating 70 μM $oMet_0$ AS in 50 mM ammonium acetate, pH 7.0, 2 mM DA for 72 h at 37 °C under mild agitation. The resulting sample was buffer exchanged using 7k MWCO *Zeba Spin* desalting columns (Thermo Fisher Scientific) with elution in 50 mM ammonium acetate, pH 7.0. $oMet_0$ and $oMet_4$ AS were mixed at final equimolar concentrations (20 μM) and analyzed by nano-ESI-(IM)-MS in the presence of 3 mM DA or 150 μM EGCG.

Nano-ESI-(IM)-MS measurements were performed on a Synapt G2 HDMS (Waters, Manchester, UK) equipped with a nano-ESI sample source. Home-made gold-coated borosilicate capillaries were used to infuse the samples at room temperature. The main instrumental settings were: capillary voltage, 1.5–1.8 kV; sampling cone, 25 V; extraction cone, 1 V; trap, CE 4 V; transfer, CE 0 V; trap bias, 42 V. Gas pressures used throughout the instrument were: source, 2.8 mbar; trap cell, 2.4×10^{-2} mbar; IM cell, 3.0 mbar; transfer cell, 2.5×10^{-2} mbar. Spectra were analyzed using Masslynx version 4.1 and Driftscope version 2.3 (Waters, Manchester, UK).

Author contributions—E. P., A. D. P., L. C., A. N., R. R., R. M., A. K., and C. S. data curation; E. P., A. D. P., L. C., A. N., R. R., R. M., A. K., and J. N. investigation; A. D. P., A. K., F. S., P. M., C. S., and R. G. conceptualization; A. D. P., L. C., A. N., R. R., R. M., A. K., J. N., G. A. L., F. S., P. M., C. S., and R. G. methodology; A. D. P., A. N., F. S., P. M., C. S., and R. G. writing-original draft; L. C., A. N., and C. S. formal analysis; J. N. and G. A. L. resources; G. A. L., F. S., P. M., C. S., and R. G. supervision; G. A. L., F. S., P. M., and R. G. funding acquisition; R. G. project administration.

Acknowledgment—The Synapt HDMS mass spectrometer was funded by a grant from the Hercules Foundation (Flanders).

References

1. Habchi, J., Tompa, P., Longhi, S., and Uversky, V. N. (2014) Introducing protein intrinsic disorder. *Chem. Rev.* **114,** 6561–6588 CrossRef Medline
2. Breydo, L., Wu, J. W., and Uversky, V. N. (2012) α-Synuclein misfolding and Parkinson's disease. *Biochim. Biophys. Acta* **1822,** 261–285 CrossRef Medline
3. Lautenschläger, J., Kaminski, C. F., and Kaminski Schierle, G. S. (2017) α-Synuclein: regulator of exocytosis, endocytosis, or both? *Trends Cell Biol.* **27,** 468–479 CrossRef Medline
4. Spillantini, M. G., and Goedert, M. (2018) Neurodegeneration and the ordered assembly of α-synuclein. *Cell Tissue Res.* **373,** 137–148 CrossRef Medline
5. Schildknecht, S., Gerding, H. R., Karreman, C., Drescher, M., Lashuel, H. A., Outeiro, T. F., Di Monte, D. A., and Leist, M. (2013) Oxidative and nitrative α-synuclein modifications and proteostatic stress: implications for disease mechanisms and interventions in synucleinopathies. *J. Neurochem.* **125,** 491–511 CrossRef Medline
6. Bisaglia, M., Mammi, S., and Bubacco, L. (2009) Structural insights on physiological functions and pathological effects of α-synuclein. *FASEB J.* **23,** 329–340 CrossRef Medline
7. Uversky, V. N., Yamin, G., Souillac, P. O., Goers, J., Glaser, C. B., and Fink, A. L. (2002) Methionine oxidation inhibits fibrillation of human α-synuclein *in vitro*. *FEBS Lett.* **517,** 239–244 CrossRef Medline
8. Leong, S. L., Cappai, R., Barnham, K. J., and Pham, C. L. (2009) Modulation of α-synuclein aggregation by dopamine: a review. *Neurochem. Res.* **34,** 1838–1846 CrossRef Medline
9. Nakaso, K., Tajima, N., Ito, S., Teraoka, M., Yamashita, A., Horikoshi, Y., Kikuchi, D., Mochida, S., Nakashima, K., and Matsura, T. (2013) Dop-

amine-mediated oxidation of methionine 127 in α-synuclein causes cytotoxicity and oligomerization of α-synuclein. *PloS One* **8,** e55068 CrossRef Medline
10. Leong, S. L., Pham, C. L., Galatis, D., Fodero-Tavoletti, M. T., Perez, K., Hill, A. F., Masters, C. L., Ali, F. E., Barnham, K. J., and Cappai, R. (2009) Formation of dopamine-mediated α-synuclein-soluble oligomers requires methionine oxidation. *Free Radic. Biol. Med.* **46,** 1328–1337 CrossRef Medline
11. Carmo-Gonçalves, P., Pinheiro, A. S., Romão, L., Cortines, J., and Follmer, C. (2014) UV-induced selective oxidation of Met5 to Met-sulfoxide leads to the formation of neurotoxic fibril-incompetent α-synuclein oligomers. *Amyloid* **21,** 163–174 CrossRef
12. Bengoa-Vergniory, N., Roberts, R. F., Wade-Martins, R., and Alegre-Abarrategui, J. (2017) α-Synuclein oligomers: a new hope. *Acta Neuropathol.* **134,** 819–838 CrossRef Medline
13. Hansel, A., Heinemann, S. H., and Hoshi, T. (2005) Heterogeneity and function of mammalian MSRs: enzymes for repair, protection and regulation. *Biochim. Biophys. Acta.* **1703,** 239–247 CrossRef Medline
14. Binolfi, A., Limatola, A., Verzini, S., Kosten, J., Theillet, F.-X., Rose, H. M., Bekei, B., Stuiver, M., van Rossum, M., and Selenko, P. (2016) Intracellular repair of oxidation-damaged α-synuclein fails to target C-terminal modification sites. *Nat. Commun.* **7,** 10251 CrossRef Medline
15. Rodriguez, A. R., Kramer, J. R., and Deming, T. J. (2013) Enzyme-triggered cargo release from methionine sulfoxide containing copolypeptide vesicles. *Biomacromolecules* **14,** 3610–3614 CrossRef Medline
16. Rekas, A., Knott, R. B., Sokolova, A., Barnham, K. J., Perez, K. A., Masters, C. L., Drew, S. C., Cappai, R., Curtain, C. C., and Pham, C. L. (2010) The structure of dopamine induced α-synuclein oligomers. *Eur. Biophys. J.* **39,** 1407–1419 CrossRef Medline
17. De Franceschi, G. D., Fecchio, C., Sharon, R., Schapira, A. H. V., Proukakis, C., Bellotti, V., and de Laureto, P. P. (2017) α-Synuclein structural features inhibit harmful polyunsaturated fatty acids oxidation, suggesting roles in neuroprotection. *J. Biol. Chem.* **292,** 6927–6937 CrossRef Medline
18. Maltsev, A. S., Chen, J., Levine, R. L., and Bax, A. (2013) Site-specific interaction between α-synuclein and membranes probed by NMR-observed methionine oxidation rates. *J. Am. Chem. Soc.* **135,** 2943–2946 CrossRef Medline
19. Ehrnhoefer, D. E., Bieschke, J., Boeddrich, A., Herbst, M., Masino, L., Lurz, R., Engemann, S., Pastore, A., and Wanker, E. E. (2008) EGCG redirects amyloidogenic polypeptides into unstructured, off-pathway oligomers. *Nat. Struct. Mol. Biol.* **15,** 558–566 CrossRef Medline
20. Konijnenberg, A., Ranica, S., Narkiewicz, J., Legname, G., Grandori, R., Sobott, F., and Natalello, A. (2016) Opposite structural effects of epigallocatechin-3-gallate and dopamine binding to α-synuclein. *Anal. Chem.* **88,** 8468–8475 CrossRef Medline
21. Kim, H.-S., Quon, M. J., and Kim, J.-A. (2014) New insights into the mechanisms of polyphenols beyond antioxidant properties: lessons from the green tea polyphenol, epigallocatechin 3-gallate. *Redox Biol.* **2,** 187–195 CrossRef Medline
22. Coskuner, O., and Wise-Scira, O. (2013) Arginine and disordered amyloid-β peptide structures: molecular level insights into the toxicity in Alzheimer's disease. *ACS Chem. Neurosci.* **4,** 1549–1558 CrossRef Medline
23. Bertoncini, C. W., Rasia, R. M., Lamberto, G. R., Binolfi, A., Zweckstetter, M., Griesinger, C., and Fernandez, C. O. (2007) Structural characterization of the intrinsically unfolded protein β-synuclein, a natural negative regulator of α-synuclein aggregation. *J. Mol. Biol.* **372,** 708–722 CrossRef Medline
24. Herrera, F. E., Chesi, A., Paleologou, K. E., Schmid, A., Munoz, A., Vendruscolo, M., Gustincich, S., Lashuel, H. A., and Carloni, P. (2008) Inhibition of α-synuclein fibrillization by dopamine is mediated by interactions with five C-terminal residues and with E83 in the NAC region. *PloS One* **3,** e3394 CrossRef Medline
25. Norris, E. H., Giasson, B. I., Hodara, R., Xu, S., Trojanowski, J. Q., Ischiropoulos, H., and Lee, V. M. (2005) Reversible inhibition of α-synuclein fibrillization by dopaminochrome-mediated conformational alterations. *J. Biol. Chem.* **280,** 21212–21219 CrossRef Medline
26. Mazzulli, J. R., Armakola, M., Dumoulin, M., Parastatidis, I., and Ischiropoulos, H. (2007) Cellular oligomerization of α-synuclein is determined by the interaction of oxidized catechols with a C-terminal sequence. *J. Biol. Chem.* **282,** 31621–31630 CrossRef Medline
27. Natalello, A., Benetti, F., Doglia, S. M., Legname, G., and Grandori, R. (2011) Compact conformations of α-synuclein induced by alcohols and copper. *Proteins* **79,** 611–621 CrossRef Medline
28. Barth, A. (2007) Infrared spectroscopy of proteins. *Biochim. Biophys. Acta* **1767,** 1073–1101 CrossRef
29. Vitali, M., Rigamonti, V., Natalello, A., Colzani, B., Avvakumova, S., Brocca, S., Santambrogio, C., Narkiewicz, J., Legname, G., Colombo, M., Prosperi, D., and Grandori, R. (2018) Conformational properties of intrinsically disordered proteins bound to the surface of silica nanoparticles. *Biochim. Biophys. Acta* **1862,** 1556–1564 CrossRef Medline
30. Ami, D., Ricagno, S., Bolognesi, M., Bellotti, V., Doglia, S. M., and Natalello, A. (2012) Structure, stability, and aggregation of β-2 microglobulin mutants: insights from a Fourier transform infrared study in solution and in the crystalline state. *Biophys. J.* **102,** 1676–1684 CrossRef Medline
31. Natalello, A., and Doglia, S. M. (2015) Insoluble protein assemblies characterized by Fourier transform infrared spectroscopy. *Methods Mol. Biol.* **1258,** 347–369 CrossRef Medline
32. Pivato, M., De Franceschi, G., Tosatto, L., Frare, E., Kumar, D., Aioanei, D., Brucale, M., Tessari, I., Bisaglia, M., Samori, B., de Laureto, P. P., and Bubacco, L. (2012) Covalent α-synuclein dimers: chemico-physical and aggregation properties. *PloS One* **7,** e50027 CrossRef Medline
33. Kjaergaard, M., Nørholm, A.-B., Hendus-Altenburger, R., Pedersen, S. F., Poulsen, F. M., and Kragelund, B. B. (2010) Temperature-dependent structural changes in intrinsically disordered proteins: formation of α-helices or loss of polyproline II? *Protein Sci.* **19,** 1555–1564 CrossRef Medline
34. Sang, S., Lambert, J. D., Ho, C.-T., and Yang, C. S. (2011) The chemistry and biotransformation of tea constituents. *Pharmacol. Res.* **64,** 87–99 CrossRef Medline
35. Devika, P. T., and Stanely Mainzen Prince, P. (2008) (−)-Epigallocatechin-gallate (EGCG) prevents mitochondrial damage in isoproterenol-induced cardiac toxicity in albino Wistar rats: a transmission electron microscopic and *in vitro* study. *Pharmacol. Res.* **57,** 351–357 CrossRef Medline
36. Arakawa, H., Maeda, M., Okubo, S., and Shimamura, T. (2004) Role of hydrogen peroxide in bactericidal action of catechin. *Biol. Pharm. Bull.* **27,** 277–281 CrossRef Medline
37. Zhou, W., Long, C., Reaney, S. H., Di Monte, D. A., Fink, A. L., and Uversky, V. N. (2010) Methionine oxidation stabilizes non-toxic oligomers of α-synuclein through strengthening the auto-inhibitory intra-molecular long-range interactions. *Biochim. Biophys. Acta* **1802,** 322–330 CrossRef Medline
38. Legge, F. S., Binger, K. J., Griffin, M. D., Howlett, G. J., Scanlon, D., Treutlein, H., and Yarovsky, I. (2009) Effect of oxidation and mutation on the conformational dynamics and fibril assembly of amyloidogenic peptides derived from apolipoprotein C-II. *J. Phys. Chem. B* **113,** 14006–14014 CrossRef Medline
39. Celej, M. S., Sarroukh, R., Goormaghtigh, E., Fidelio, G. D., Ruysschaert, J.-M., and Raussens, V. (2012) Toxic prefibrillar α-synuclein amyloid oligomers adopt a distinctive antiparallel β-sheet structure. *Biochem. J.* **443,** 719–726 CrossRef Medline
40. Latawiec, D., Herrera, F., Bek, A., Losasso, V., Candotti, M., Benetti, F., Carlino, E., Kranjc, A., Lazzarino, M., Gustincich, S., Carloni, P., and Legname, G. (2010) Modulation of α-synuclein aggregation by dopamine analogs. *PloS One* **5,** e9234 CrossRef Medline
41. Ami, D., Natalello, A., and Doglia, S. M. (2012) Fourier transform infrared microspectroscopy of complex biological systems: from intact cells to whole organisms. *Methods Mol. Biol.* **895,** 85–100 CrossRef Medline
42. Susi, H., and Byler, D. M. (1986) Resolution-enhanced Fourier transform infrared spectroscopy of enzymes. *Methods Enzymol.* **130,** 290–311 CrossRef Medline
43. Laemmli, U. K. (1970) Cleavage of structural proteins during the assembly of the head of bacteriophage T4. *Nature* **227,** 680–685 CrossRef Medline

Methionine oxidation in α-synuclein inhibits its propensity for ordered secondary structure

Erika Ponzini, Antonella De Palma, Lucilla Cerboni, Antonino Natalello, Rossana Rossi, Rani Moons, Albert Konijnenberg, Joanna Narkiewicz, Giuseppe Legname, Frank Sobott, PierLuigi Mauri, Carlo Santambrogio and Rita Grandori

J. Biol. Chem. 2019, 294:5657-5665.
doi: 10.1074/jbc.RA118.001907 originally published online February 12, 2019